IEEE Photonics Journal
An IEEE Photonics Society Publication

Open Access

A Liquid-Level Sensing Technique Based on Differential Detection of Correlation Peaks From Broadband Chaos

Volume 9, Number 5, October 2017

Heng Yi
Li Xia
Jun Xu
Can Yu
Ying Wu
Chen Li
Lin Zhu

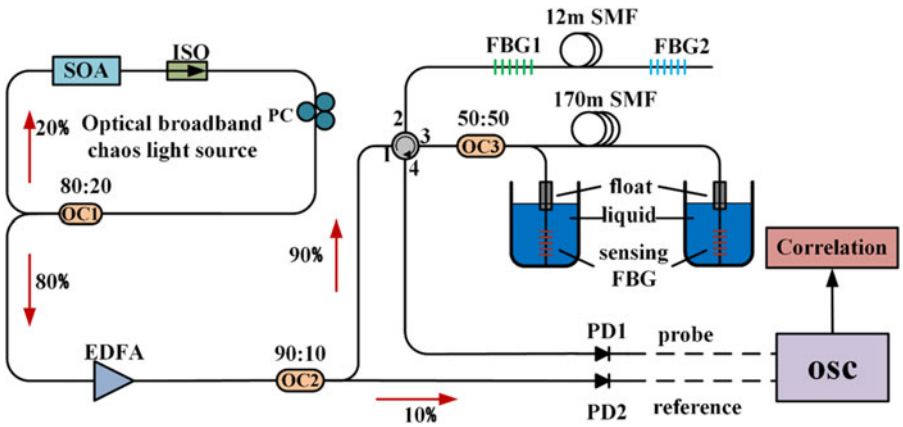

DOI: 10.1109/JPHOT.2017.2732681
1943-0655 © 2017 IEEE

A Liquid-Level Sensing Technique Based on Differential Detection of Correlation Peaks From Broadband Chaos

Heng Yi,[1] Li Xia,[1,2] Jun Xu,[1,2] Can Yu,[1] Ying Wu,[1] Chen Li,[1] and Lin Zhu[3]

[1]School of Optical and Electronic Information, Huazhong University of Science and Technology, Wuhan 430074, China
[2]Wuhan National Laboratory for Optoelectronics, Wuhan 430074, China
[3]Holcombe Department of Electrical and Computer Engineering, Clemson University, Clemson, SC 29634 USA

DOI:10.1109/JPHOT.2017.2732681
1943-0655 © 2017 IEEE. Translations and content mining are permitted for academic research only. Personal use is also permitted, but republication/redistribution requires IEEE permission. See http://www.ieee.org/publications_standards/publications/rights/index.html for more information.

Manuscript received June 30, 2017; revised July 11, 2017; accepted July 24, 2017. Date of publication July 28, 2017; date of current version August 8, 2017. This work was supported in part by the sub-Project of the Major Program of the National Natural Science Foundation of China under Grant 61290315 and in part by the National Natural Science Foundation of China under Grants 61675078 and 61290311.
Corresponding authors: Li Xia; Jun Xu (xiali@hust.edu.cn; xujun@mail.hust.edu.cn).

Abstract: A highly sensitive liquid-level sensing technique is proposed and experimentally demonstrated. Two narrowband fiber Bragg gratings (FBGs) with high reflectivity are used to filter out the two light signals from the broadband chaos. Two weak FBGs are served respectively as the liquid-level sensors at two different sensing points. The change of liquid-level will induce the wavelength shift of the weak FBGs, which can be demodulated through calculating the amplitude difference in the logarithm of two cascaded correlation peaks in the cross-correlation spectrum. Adopting the differential calculation of the cascaded correlation peak amplitudes can avoid the complex wavelength detection and enhance the robustness against the power variation of the broadband chaos. Our method can also support the simultaneous multiplexing and locating with high resolution from the time delays of the corresponding correlation peaks. Experimental results show that the liquid level changes linearly with the relative peak amplitude difference in the logarithm and the sensitivity is around 0.019/mm. The sensing resolution of liquid-level can reach at least 3 mm, and the relative resolution is around 0.055. Moreover, the real-time fiber fault monitoring can be achieved with a spatial resolution of around 2.8 cm, which improves the survivability in harsh environment.

Index Terms: Fiber Bragg gratings, fiber optics sensors, multiplexing, Chaos, liquid level.

1. Introduction

Liquid level sensing is important for many industrial applications, such as fuel storage and biochemical system [1], [2]. There are different kinds of liquid level sensing techniques based on electrical [3], mechanical [4], microwave-photonic [5] and optical methods [6], [7]. For example, microwave-photonic sensor based on chaotic laser has a lot of advantages such as the remote water-level monitoring and large measurement range [5]. But its sensing resolution is only 2 cm, which is not suitable for some applications requiring the high-resolution detection. In addition, the microwave-photonic sensors are vulnerable to electromagnetic interference. Electrical liquid level sensors are

widely employed, but they are potentially explosive or erosive [8]. Optical fiber sensors offer many advantages due to their intrinsic properties [9]. However, some of the liquid level detection methods based on optical fibers need complex structures such as single-mode-multimode-thinned-single-mode (SMTS) waveguides, and the liquid level measurement range is only 9 mm [10]. Some methods need special treatment like etching, which adds the costs and production difficulty [11]. The liquid sensor based on D-shaped optical fibers has a high measurement resolution, which is 1 mm. But the sensing technique highly depends on the environmental stability. Any micro-bend of the fiber or temperature variation will change the measurement results considerably. In addition, it does not have the ability to locate the fault in the sensing network [12]. Recently, Fiber Bragg grating (FBG) based distributed optical sensing network has attracted extensive attention due to its significant advantages of erosion resistance, immunity to electromagnetic interference, compactness, excellent multiplexing capability, low cost, and mature manufacture [13]–[15]. Several Fiber Bragg grating based liquid level sensors have been reported, but most of them are wavelength demodulated. This demodulation method is based on the wavelength sweeping that requires extra sweeping time. Especially in multipoint measurements, monitoring the wavelength shifts of all the FBGs is difficult to implement due to the bandwidth limitation of the light source [16]. The long period grating (LPG) has been utilized as an optical edge filter to convert the FBG's wavelength shift induced by the strain into the received optical power change [17]. But for such an intensity demodulation system, the power variation of the light source or the loss variation of the transmission system can lead to unstable results, especially for the high precision sensing applications. It is not possible for this intensity demodulation system to differentiate the power change induced by the wavelength shift from the light source power variation. Thus, an Intensity demodulation incorporated with the appropriate optical filter and novel interrogation scheme should be proposed to resist the light power variation in sensing network.

In the actual fiber-optic sensing network, fiber fault could happen occasionally, which presents a significant challenge for the whole system [18]. Recently, optical chaos has attracted more and more attention for fiber-optic sensing due to its excellent advantages in precise fault location [19]. In our previous work, simultaneous and precise fiber fault location in the wavelength division multiplexing – passive optical network (WDM-PON) is implemented based on optical broadband chaos. Through applying cross-correlation algorithm to the reference signal and Fresnel reflection signal of the fiber fault, precise locating of the fiber fault can be obtained [20]. In the large scale distributed sensor network such as water level detection in dams, rivers and lakes, real-time breakpoint fault monitoring is very important. It can save a lot of manpower and time to pinpoint the breakpoint fault, thus improving its efficiency and survivability in harsh environment.

In this work, a new demodulation method based on the optical broadband chaos and differential calculation is proposed to achieve the liquid level measurement. The proposed scheme supports the simultaneous multiplexing and locating with high resolution. A weak FBG is attached to a float, which converts the liquid level changes to the wavelength shift. Then by adopting the differential calculation, the liquid level information is obtained from the difference in the logarithm of the two correlation peak amplitudes. We also demonstrate that the proposed sensing technique is robust against the light source power variation.

2. Schematic Diagram and Principle

The schematic diagram of the liquid level sensing network is shown in Fig. 1. The whole system consists of two parts: the broadband chaotic light source and the liquid level sensing device. A semiconductor optical amplifier (SOA) ring structure with an isolator (ISO) is used to create the chaotic light source. The SOA (Model: S7FC1013S) has the parameters of the central wavelength (1550 nm), optical bandwidth (74 nm), saturation output power (14 mw), and small signal gain (13 dB). The isolator and the polarization controller (PC) are used to obtain unidirectional propagation and appropriate polarization state, respectively. An 80:20 optical coupler (OC1) provides 20% feedback light and 80% output light. An erbium doped fiber amplifier (EDFA) acts as a pre-amplifier for sensing power boost. Then a 90:10 optical coupler (OC2) provides 10% transmission light as

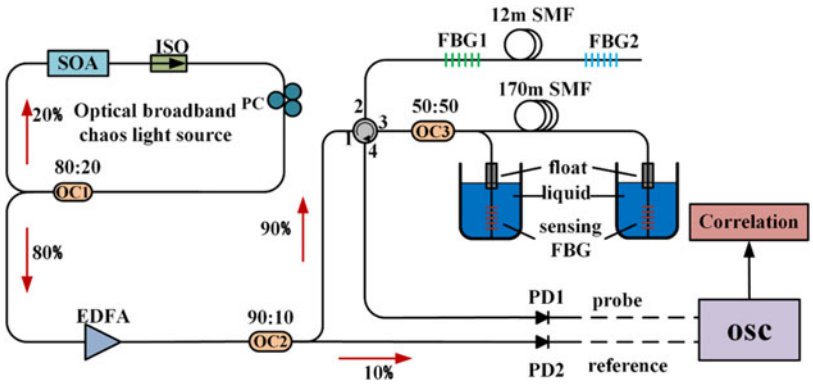

Fig. 1. The schematic of the highly sensitive liquid-level sensing system.

the reference signal and 90% transmission light as the probe signal. The reference signal is directly detected, and the probe signal is launched into the liquid level sensing device through a circulator. Two photodetectors (PDs) with 1 GHz bandwidth are used in the correlation detection. An optical spectrum analyzer (Yokogawa AQ6370C) is used to measure the optical spectrum. A real-time oscilloscope (OSC) with 12.5 GHz bandwidth and 50 GSa/s sampling rate is used to record the changes of reference signal and probe signal.

In the liquid level sensing device, the probe light is first sent into two cascaded narrow bandwidth FBGs via a 4-port circulator, which acts as filter FBGs. Narrow spectrum reflections are created by these two gratings, and then directed to a 50:50 optical coupler (OC3), which divides the probe light into two branches for multipoint liquid level sensing. In order to distinguish the two branches in the time-domain, 170 m single mode fiber (SMF) is inserted to create a time delay between the two branches. At each branch, there is a sensing unit consisting of a weak broadband FBG attached to a cylinder shape float. Then the reflected signals of the two branches pass through the circulator and are collected by a PD. The power of the reflected signal is in proportion to the overlap integral between the reflection spectrum of the filtering FBGs and that of the sensing FBGs.

The sensing operation principle is shown in Fig. 2. First, the broad spectrum chaotic light passes through the two narrowband FBGs, A1 and A2, and the reflection spectrums are shown in Fig. 2(a). When the center wavelength of sensing grating (broadband FBG) shifts $\Delta\lambda$, as shown in Fig. 2(b), the area of overlap between the reflection spectrum will change, as shown in Fig. 2(c), which leads to the change of the power detected by PDs, as shown in Fig. 2(e) and (f). Fig. 2(g) shows the cross-correlation spectrum of A1 and A2. As we know, by adopting the cross-correlation algorithm to the reference and probe signal, the measured sensing response and precise locating can be simultaneously interrogated, where the peak location indicates the position of the sensing point, and the peak amplitude shows the sensing information [13]. Due to the around 12 m time delay line between the two filter FBGs, after the cross-correlation operation, there will be two correlation peaks for each sensing point. Each peak corresponds to one filter FBG, as shown in Fig. 2(g), P_{A_1} and P_{A_2} are the correlation amplitudes of the two peaks related to the narrowband FBG1 and FBG2, respectively. After the differential detection of the correlation peaks, there is a linear relationship between the difference in the logarithm of the amplitudes of correlation peaks and the wavelength shift, as shown in Fig. 2(h). The amplitudes of the correlation peaks in the cross-correlation are proportional to the overlap between the reflected spectrums by the filter FBGs and the broadband sensing FBG, respectively.

In the sensing unit, as illustrated in Fig. 1, one end of the sensing FBG is fixed to the bottom of the container, and the other end is attached to a float which can transfer buoyancy into the axial strain on the fiber. Thus, the change of the liquid level can cause the wavelength shift of the weak broadband FBG reflection spectrum. The sensing principle can thus be derived from the following equations:

$$F_{float} = F_B + mg \tag{1}$$

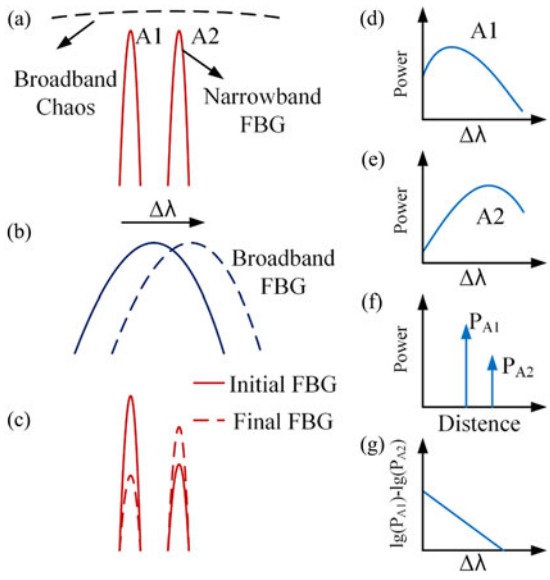

Fig. 2. The operation principle: (a) Broadband chaos and narrow FBG, (b) broadband FBG, (c) the waveform filtered by broadband FBG, (e) plot of power responses of A1, (f) plot of power responses of A2, (g) cross-correlation spectrum of A1 and A2, (h) plot of the subtraction result of these two responses A1 and A2.

Where F_{float} is the buoyancy on the float, m is the mass of the float, g is the gravity acceleration, and F_B is the tension on the weak broadband FBG.

The buoyancy of the float can be expressed as:

$$F_{float} = \rho g \left(\Delta h + h_0\right) S \tag{2}$$

Where ρ is the density of the liquid, $(\Delta h + h_0)$ is the height of the submerged part of the float's body, h_0 is the original height where the gravity and buoyancy are just in balance, Δh is the liquid level change to be measured, and S is the base area of the float. When the liquid level is h_0, F_B is just zero. Take this liquid level as the starting point for measurement. Thus, we can get the relationship:

$$F_B \propto \Delta h \tag{3}$$

According to (2), the change of the liquid level induces the change of the buoyancy F_{float}. Thus, the tension F_B changes correspondingly, which causes the shift of the reflection spectrum of the sensing FBG. It is well known that in a certain stress range, there is a linear relationship between the wavelength shift $\Delta\lambda$ and the applied stress.

According to (3), there will also be a linear relationship between Δh and $\Delta\lambda$. As mentioned above, the output power of the PD is proportional to the overlap between the reflection spectrum of the two filter FBGs and that of the sensing FBG.

The wavelength dependent power reflection coefficient ($R(\lambda)$) of weak broadband sensing FBG can be approximately modeled as Gaussian [21]:

$$R\left(\lambda\right) \propto \exp\left(-4\ \ln\left(2\left(\frac{\lambda - \left(\lambda_{B_0} + \Delta\lambda\right)}{B}\right)^2\right)\right) \tag{4}$$

Where λ_{B_o} is the initial center wavelength of the grating, and $\Delta\lambda$ is the wavelength shift, and B is the full width at half maximum (FWHM).

For the filters, because the bandwidth of the filter FBGs are very narrow, they can be approximated as a single wavelength model. We define the center wavelength of narrowband FBGs as the approximate single wavelength, which is λ_1 and λ_2, respectively. So, the power spectral densi-

ties at the two wavelengths on the reflection spectrum of the sensing FBG represent the powers corresponding to two narrowband FBGs.

Thus, the powers for the two wavelengths ($P\lambda_1(\Delta\lambda)$ and $P\lambda_2(\Delta\lambda)$) can be expressed as two Gaussian functions [21]:

$$P_{\lambda_1}(\Delta\lambda) \propto \exp\left(-4\ln\left(2\left(\frac{\lambda_1 - (\lambda_{B_0} + \Delta\lambda)}{B}\right)^2\right)\right) \tag{5}$$

$$P_{\lambda_2}(\Delta\lambda) \propto \exp\left(-4\ln\left(2\left(\frac{\lambda_2 - (\lambda_{B_0} + \Delta\lambda)}{B}\right)^2\right)\right) \tag{6}$$

We define the difference ($Y(\Delta\lambda)$) in the logarithm between $P_{\lambda_1}(\Delta\lambda)$ and $P_{\lambda_2}(\Delta\lambda)$ as:

$$\begin{aligned} Y(\Delta\lambda) &= lgP_{\lambda_1}(\Delta\lambda) - lgP_{\lambda_2}(\Delta\lambda) \\ &\times \propto (\lambda_1 - \lambda_2)(\lambda_1 + \lambda_2 - 2\lambda_{B_0}) - 2\Delta\lambda(\lambda_1 - \lambda_2) \end{aligned} \tag{7}$$

In the equation, $(\lambda_1 - \lambda_2)(\lambda_1 + \lambda_2 - 2\lambda_{B_o})$ and $(\lambda_1 - \lambda_2)$ will be two constant terms for the given experimental setup. And we will get the following relation: $Y(\Delta\lambda)$ and $\Delta\lambda$ are linearly related, which provides a method that turns the wavelength shift to the power difference change. According to the above discussion, $Y(\Delta\lambda)$ and Δh are also linearly related.

We can get the information of the liquid level from the difference in the logarithm of the reflection power of the two narrowband FBGs. As mentioned above, the amplitudes of the two correlation peaks in the cross-correlation spectrum are proportional to the corresponding power relative to the narrowband FBG1 and FBG2. Thus, the amplitudes of the two correlation peaks in the cross-correlation spectrum is proportional to $P_{\lambda_1}(\Delta\lambda)$ and $P_{\lambda_2}(\Delta\lambda)$, respectively. Moreover, the difference in the logarithm of the two correlation peak amplitudes P_{A_1} and P_{A_2} is linearly related to Δh. After the differential detection of the correlation peaks, there is a linear relationship between the difference in the logarithm of the amplitudes of correlation peaks and the liquid level.

3. Experiment and Discussion

Experimental studies based on the setup depicted in Fig. 1 have been conducted. In our experiment, two narrowband FBGs (FBG1, FBG2) acting as filters are centered at 1550.1 nm and 1550.8 nm with reflectivity of over 95% and 3-dB bandwidth of around 0.2 nm, as shown in Fig. 3(a). The red dashed line in Fig. 3(a) represents the power spectral density of the broadband chaotic light source. The characteristics of the broadband chaotic light have been studied in our previous work. The optical 3-dB bandwidth of the broadband is about 50 nm, and the chaotic light possesses a random up-and-down waveform in time series [13], [16]. In order to distinguish two relative amplitudes in the cross-correlation spectrum, an around 12 m fiber delay line is inserted between the two narrowband FBGs. Two same weak broadband FBGs acting as sensors (A, B) are centered at 1549.9 nm with the same reflectivity of 3% and 3-dB bandwidth of around 1.3 nm, as shown in Fig. 3(b). In the meanwhile, the fiber branch with sensor B is around 170 m longer than that with sensor A. The final waveform filtered by narrowband FBG is shown in Fig. 3(c).

After the cross-correlation operation, the correlation spectrum is shown in Fig. 4(a), where the x axis has been converted to the relative distance. Two pairs of close peaks can be clearly seen in the cross-correlation spectrum, and each pair represents one sensing point. For sensing point A, the peaks related to the narrowband FBG1 and FBG2 are A1 and A2, respectively. Similarly, for sensing point B, the peaks are B1 and B2, respectively. The distance between the two close peaks represents the actual distance between the two narrowband FBGs. As shown in Fig. 4(a), the distance between the two close peaks is 11.9 m, which matches well with the delay-line around 12 m employed. A distance of 167 m between the two pairs of peaks is the actual length difference between the two sensing branch, which also matches well with the delay-line around 170 m employed. In the meanwhile, the spatial resolution of the locating is determined by the full-width at half-maximum (FWHM) of the auto-correlation peak according to 3-dB criterion. The

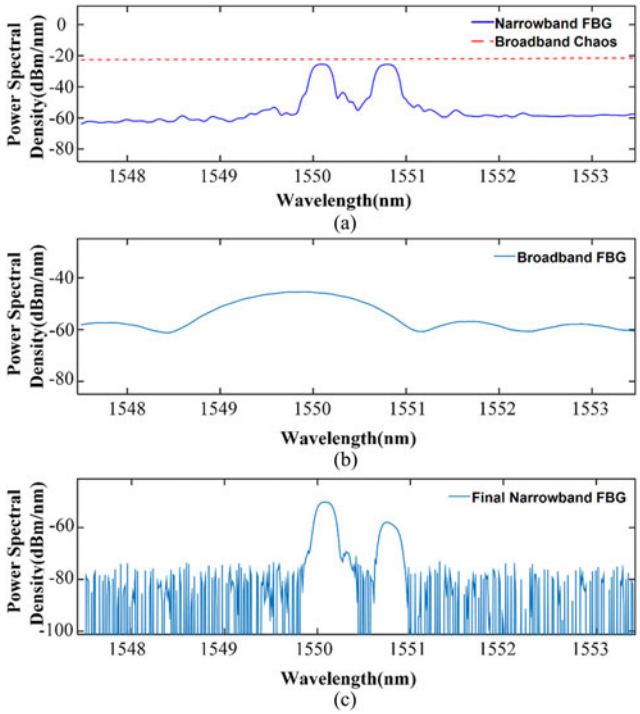

Fig. 3. The input spectra: (a) Broadband chaos and narrowband FBG, (b) broadband FBG, (c) the waveform filtered by narrowband FBG.

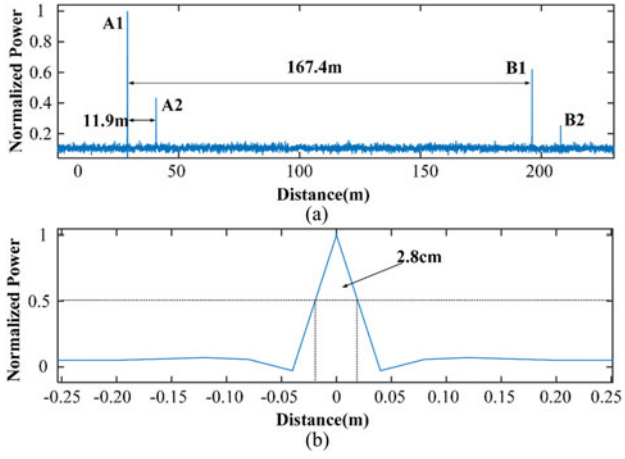

Fig. 4. (a) Cross-correlation spectrum of a certain liquid level. (b) FWHM of the auto-correlation spectrum with a spatial resolution of 2.8 cm.

FWHM is related to the bandwidth of the chaotic signal. As shown in the Fig. 4(b), the spatial resolution is about 2.8 cm.

After calculating the normalized difference (peak to peak ratio, PPR) in the logarithm between the two peaks in each pair, the relationship between the liquid level and the PPR is shown in Fig. 5(a) and (b). In our experiment, the liquid level is adjusted by injecting liquid into the water tank in a step of 3 mm. As the liquid level changes from 0 to 54 mm, the PPR of both sensing units changes linearly. The linearity (R^2) is 0.99653 and 0.98975, respectively. And the sensitivity of two sensor point is 0.01924 /mm and 0.01885 /mm, which are almost the same, because we use two floats of the similar shape and size in the experiment. Then, the difference between the real liquid level measurement and the linear fit data at Point A and Point B are shown in Fig. 5(c) and (d),

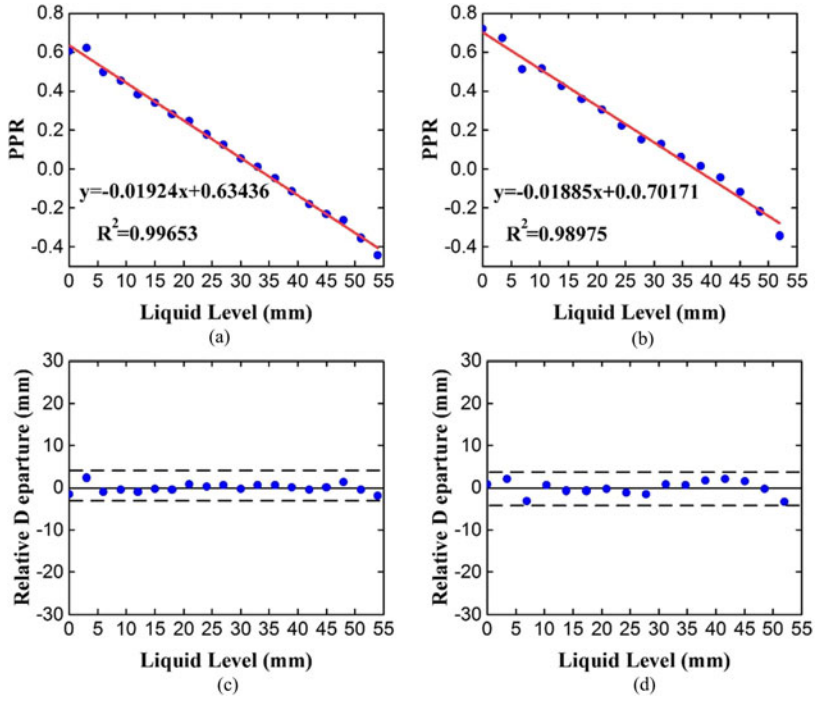

Fig. 5. The relationship between the liquid level and the PPR: (a) Subtraction result of the power A1 and power A2 versus water level variation, (b) subtraction result of the power B1 and power B2 versus water level variation, (c) the difference between the real level measurement and the linear fit data at Point A, (d) the difference between the real level measurement and the linear fit data at Point B.

respectively. For sensor point A, the error is within ±2.3 mm. For sensor point B, the error is within ±2.5 mm. As shown in Fig. 5(a) and (b), when the liquid level changes 3 mm, the PPR changes are obvious. So, the sensing resolution of liquid level can reach at least 3 mm. The relative resolution is defined as the ratio of the actual resolution (3 mm) to measurement range (54 mm), which is around 0.055.

The liquid level sensing range is 54 mm in our experiment. The sensing range is determined by many factors, such as the bandwidth of weak broadband FBG, the base area of the float, and the density of the liquid. For example, as shown in Fig. 2(b), the change of the liquid level leads to the wavelength shift of the weak broadband FBG reflection spectrum. Thus, if the bandwidth of weak FBG is wider, it will provide more room for the center wavelength change and result in a larger sensing range.

Another advantage of adopting the differential calculation is its robustness against the power variation from the broadband chaos. For an intensity demodulation system, the power variation of the light source or the loss variation of the system such as fiber bend loss presents significant challenges, which may lead to unstable results. This can easily happen in the large scale distributed measurements.

The impact of source fluctuations on the measurement has been investigated. We decrease the power of the light source by 2.6 dBm, and then compare the normalized sensor responses obtained before and after the power decrease. The results are shown in Fig. 6. Fig. 6(a) shows the original response, while Fig. 6(b) represents the response after the test. As shown in Fig. 6(b), the peak amplitudes drop significantly, which is apparently due to the reduction of the optical source power. Although the normalized power becomes lower after the source power is reduced, the ratio between the two relative peaks in the correlation spectrum will remain unchanged. After calculation, the PPR are 0.364 and 0.358, respectively. So, despite the considerable changes of the peak values, the PPR remains almost unchanged during the source power change.

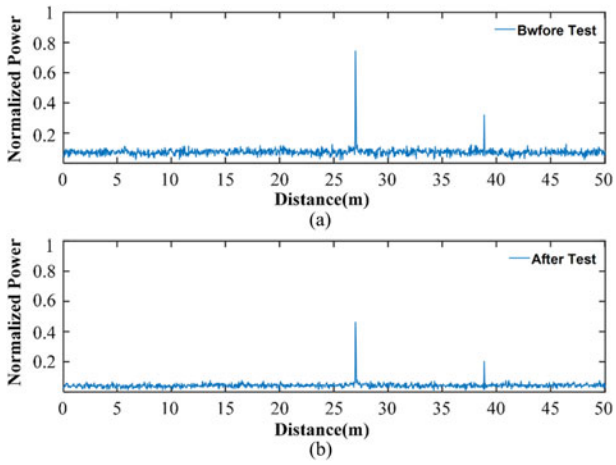

Fig. 6. Comparison of the normalized system time-domain responses before (a) and after (b).

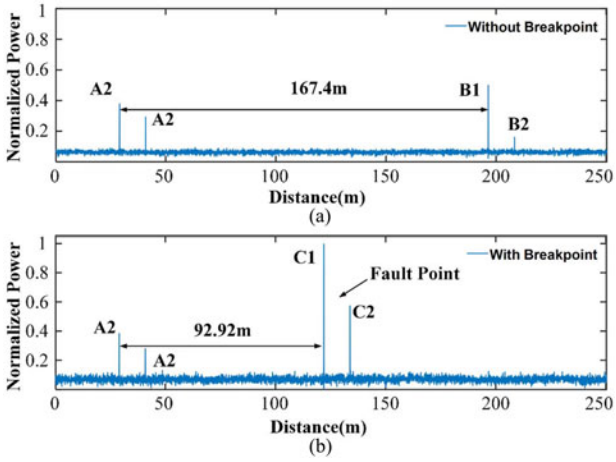

Fig. 7. Experiment results of the real-time fiber fault monitoring: (a) Without breakpoint, (b) with breakpoint.

At last, the experiment of real-time fiber fault monitoring is implemented. In the experiment, we cut off the branch with sensor B at around 90 m from the optical coupler 3. As shown in Fig. 7(b), the peak B1 and peak B2 disappear and two fiber breakpoints of C1 and C2 peaks appear in the correlation spectrum. These peaks can be easily distinguished due to their different positions in the correlation spectrum. Compared with the peak amplitude B1 and B2 shown in Fig. 7(a), the C1 and C2 peaks are significantly higher. This is because the reflection of the weak broadband FBG is only 3%, while the reflection of the end of the fiber is about 4%. Moreover, the reflection spectrum of the broadband FBG is not uniform, and the center wavelength of narrowband FBG may be located at the lossy side of the spectrum of broadband FBG. This also leads to the reduced power. In the unaffected branch with sensor A, the peaks A1 and A2 remain unchanged. Through the peak searching algorithm, precise locating of the breakpoints can be pinpointed with a spatial resolution of 2.8 cm.

It is noted that the fiber fault occurring in one sensing line will not impede the operation in other sensing lines, and the precise pinpoint of the fiber breakpoints can be implemented without extra manpower and waiting time. Consequently, the operational reliability and survivability is improved.

The temperature variation does have some impact on the sensing results. It is indeed necessary to stabilize the FBG1 and FBG2 in temperature for a better and more accurate operation in our

experiment. However, if it is not stabilized and the change of environment temperature is not very large (a few degrees), the wavelength shift of FBG1 and FBG2 will be within tens of pm. With the differential algorithm, it will result in the error of liquid-level sensing to be around 0.5 mm. This is still acceptable compared to the large measurement range.

4. Conclusion

In this work, a highly sensitive liquid-level sensing technique is proposed and experimentally demonstrated. Measurement of the liquid level is realized by the differential calculation of the amplitudes of two neighboring correlation peaks in the cross-correlation spectrum. Differential algorithm is robust against the power variation and other power losses in the sensing network. Meanwhile, real-time fiber fault monitoring with a high spatial resolution of 2.8 cm promotes survivability in harsh environment. In addition, network capacity can be greatly expanded by adding sensing branches and sensing points in one branch. Our sensing network provides great potential for the liquid level measurement in large bodies of water such as dams, rivers and lakes. Finally, this method is not limited to the liquid level sensing, but can also be used to measure other parameter such as temperature, strain, etc.

References

[1] C. Zhao, L. Ye, X. Yu, and J. Ge, "Continuous fuel level sensor based on spiral side-emitting optical fiber," *J. Control Sci. Eng.*, vol. 2012, no. 3, 2012, Art. no. 267519.

[2] P. K. Bhaba, S. Sathishbabu, A. Asokan, and T Karunanithi, "Real time implementation of Wiener Model PI (WMPI) controller in a conical tank liquid level process," *J. Appl. Sci.*, vol. 7, no. 15, pp. 2194–2197, 2007.

[3] F. Reverter, X. Li, and G. C. M. Meijer, "Liquid-level measurement system based on a remote grounded capacitive sensor," *Sens. Actuators A, Phys.*, vol. 138, no. 1, pp. 1–8, 2007.

[4] G. A. Campbell and R. Mutharasan, "Sensing of liquid level at micron resolution using self-excited millimeter sized PZT-cantilever," *Sens. Actuators A, Phys.*, vol. 122, no. 2, pp. 326–334, 2005.

[5] Y. Ji *et al.*, "Microwave-photonic sensor for remote water-Level monitoring based on chaotic laser," *Int. J. Bifurcation Chaos*, vol. 24, no. 3, pp. 393–395, 2014.

[6] A. F. Obaton, G. Laffont, C. Wang, A. Allard, and P. Ferdinand, "Tilted fiber bragg gratings and phase sensitive-optical low coherence interferometry for refractometry and liquid level sensing," *Sens. Actuators A, Phys.*, vol. 189, no. 2, pp. 451–458, 2013.

[7] T. Guo *et al.*, "Temperature-insensitive fiber Bragg grating liquid-level sensor based on bending cantilever beam," *IEEE Photon. Technol. Lett.*, vol. 17, no. 11, pp. 2400–2402, Nov. 2005.

[8] Y. Dai, Q. Sun, S. Tan, J. Wo, J. Zhang, and D. Liu, "Highly sensitive liquid-level sensor based on dual-wavelength double-ring fiber laser assisted by beat frequency interrogation," *Opt. Exp.*, vol. 20, no. 25, pp. 27367–27376, 2012.

[9] B. Lee, "Review of the present status of optical fiber sensors," *Opt. Fiber Technol.*, vol. 9, no. 2, pp. 57–79, 2003.

[10] L. Li, L. Xia, Z. Xie, and D. Liu, "All-fiber Mach-Zehnder interferometers for sensing applications," *Opt. Exp.*, vol. 20, no. 10, pp. 11109–11120, 2012.

[11] B. Yun, N. Chen, and Y. Cui, "Highly sensitive liquid-level sensor based on etched fiber Bragg grating," *IEEE Photon. Technol. Lett.*, vol. 19, no. 21, pp. 1747–1749, Nov. 2007.

[12] S. M. Chandani and N. A. F. Jaeger, "Optical fiber-based liquid level sensor," *Opt. Eng.*, vol. 46, no. 11, 2007, Art. no. 114401.

[13] Y. Luo *et al.*, "Optical chaos and hybrid WDM/TDM based large capacity quasi-distributed sensing network with real-time fiber fault monitoring," *Opt. Exp.*, vol. 23, no. 3, pp. 2416–2423, 2015.

[14] A. D. Kersey *et al.*, "Fiber grating sensors," *J. Lightw. Technol.*, vol. 15, no. 8, pp. 1442–1463, Aug. 1997.

[15] K. O. Hill and G. Meltz, "Fiber Bragg grating technology fundamentals and overview," *J. Lightw. Technol.*, vol. 15, no. 8, pp. 1263–1276, Aug. 1997.

[16] L. Xia, C. Yu, Y. Ran, J. Xu, and W. Li, "Static/dynamic strain sensing applications by monitoring the correlation peak from optical wideband chaos," *Opt. Exp.*, vol. 23, no. 20, pp. 26113–26123, 2015.

[17] V. R. Pachava, S. Kamineni, S. S. Madhuvarasu, K. Putha, and V. R. Mamidi, "FBG based high sensitive pressure sensor and its low-cost interrogation system with enhanced resolution," *Photon. Sens.*, vol. 5, no. 4, pp. 321–329, 2015.

[18] R. A. Prerz-Herrera, M. Fernandez-Vallejo, and M. Lopez-Amo, "Robust fiber-optic sensor networks," *Photon. Sens.*, vol. 2, no. 4, pp. 366–380, 2012.

[19] N. Xu *et al.*, "Fault detection technique for wavelength division multiplexing passive optical network using chaotic fiber laser," *Opt. Fiber Technol.*, vol. 20, no. 2, pp. 163–167, 2014.

[20] L. Xia, D. Huang, J. Xu, and D. Liu, "Simultaneous and precise fault locating in WDM-PON by the generation of optical wideband chaos," *Opt. Lett.*, vol. 38, no. 19, pp. 3762–3764, 2013.

[21] R. Cheng and L. Xia, "Interrogation of weak Bragg grating sensors based on dual-wavelength differential detection," *Opt. Lett.*, vol. 41, no. 22, pp. 5254–5257, 2016.